Flow Measurement and Instrumentation 46 (2015) 204–212

Contents lists available at ScienceDirect

Flow Measurement and Instrumentation

journal homepage: www.elsevier.com/locate/flowmeasinst

A new visualisation and measurement technology for water continuous multiphase flows

Mi Wang [a,*], Jiabin Jia [a,1], Yousef Faraj [a], Qiang Wang [a], Cheng-gang Xie [b], Gary Oddie [b], Ken Primrose [c], Changhua Qiu [c]

[a] University of Leeds, Leeds LS2 9JT, UK
[b] Schlumberger Gould Research, Cambridge CB3 0EL, UK
[c] Industrial Tomography Systems plc, Manchester M3 3JZ, UK

ARTICLE INFO

Article history:
Received 1 December 2014
Received in revised form
2 May 2015
Accepted 18 June 2015
Available online 6 July 2015

Keywords:
Tomography
Multiphase flows
Visualisation
Metering

ABSTRACT

This paper reports the performance of a research prototype of a new multiphase flow instrument to non-invasively measure the phase flow rates, with the capability to rapidly image the flow distributions of two- and three-phase (gas and/or oil in water) flows. The research prototype is based on the novel concepts of combining vector Electrical Impedance Tomography (EIT) sensor (for measuring dispersed-phase velocity and fraction) with an electromagnetic flow metre (EMF, for measuring continuous-phase velocity with the EIT input) and a gradiomanometer flow-mixture density metre (FDM), in addition to on-line water conductivity, temperature and absolute pressure measurements. EIT–EMF–FDM data fusion embedded in the research prototype, including online calibration/compensation of conductivity change due to the change of fluids' temperature or ionic concentration, enables the determination of mean concentration, mean velocity and hence the mean flow rate of each individual phase based on the measurement of dispersed-phase distributions and velocity profiles. Results from first flow-loop experiments conducted at Schlumberger Gould Research (SGR) will be described. The performance of the research prototype in flow-rate measurements are evaluated by comparison with the flow-loop references. The results indicate that optimum performance of the research prototype for three-phase flows is confined within the measuring envelope 45–100% Water-in-Liquid Ratio (WLR) and 0–45% Gas Volume Fraction (GVF). Within the scope of this joint research project funded by the UK Engineering & Physical Sciences Research Council (EPSRC), only vertical flows with a conductive continuous liquid phase will be addressed.

1. Introduction

The advent of surface multiphase flowmeter (MPFM) is fundamentally changing the production monitoring of complex flows from oil–gas production wells. This transformation is driven by new technology to measure rapid variations in oil–water–gas multiphase flows equivalent or better than conventional separators. The capability to measure multiphase flow rate in real time increases operational efficiency, saving both time and cost. Accurately quantifying individual fluid phases in a production stream allows operators to make more informed decisions about well performance, to better identify, understand and remediate problematic wells, optimise artificial lift operations and build dynamic reservoir models [19].

Commonly used methods for measuring multiphase flows are based on γ-ray attenuation, RF/microwave and/or electrical impedance techniques in combination with a differential-pressure device such as a Venturi flowmeter [15,19]. Phase fraction measurement based on γ-ray attenuation methods is elegant; there are however practical or logistical difficulties to overcome when an intense radiation source is used to achieve the temporal resolution at the expense of increasing safety precautions [16]. An MPFM based on nuclear magnetic resonance (NMR) technique is currently under development [1], but an NMR system tends to be complex and expensive and has limitation in temporal resolution and hence in velocity measurement-range. Commercial available inline MPFMs can achieve approximately 5–10% flow-rate measurement accuracy for reservoir management and 2–5% for production allocation [5]. A relatively low-cost, radioactive-source

* Corresponding author.
E-mail address: m.wang@leeds.ac.uk (M. Wang).
[1] Current address: School of Engineering, University of Edinburgh, Edinburgh EH9 3JL, UK.

http://dx.doi.org/10.1016/j.flowmeasinst.2015.06.022

free MPFM is desirable for industrial applications and is the focus of this research work.

Electrical Impedance Tomography (EIT) has been developed to image and measure industrial processes with material conductivity contrast and with the continuous phase being electrically conductive [14]. Since EIT can detect local changes in electrical conductivity, the technique is used to study the unsteady mixing [8] or flow dynamics of liquid mixtures such as gas–liquid and solid–liquid mixtures [18]. EIT may, therefore, be suitable for numerous aqueous-based processes [20]. Using sequences of images obtained from a dual-plane EIT flow sensor, the local flow velocity of the dispersed phase(s) can be deduced based on pixel–pixel cross-correlation methods [11,13,3]. This demands an EIT system to have a rapid response time [18] in order to measure multiphase flows with phase distributions changing in space and time. An EIT system can be made low costs in both installation and maintenance. However, due to the nonlinear nature of the low frequency electric field distribution and the limited number of measurements (a trade-off with high measurement speed), an EIT system presents a low spatial resolution and non-uniform sensitivity distribution over the domain to be imaged. Since spatial- and time-averaged phase flow rates are the dominant parameters in multiphase flow measurement, an EIT is considered to be a good candidate for the fraction and/or velocity measurement of dispersed phases, e.g. gas- and/or oil-in-water.

2. Concepts and methods

The principle of the proposed three-phase measurement system is based on the use of multi-modality sensors and multi-dimensional data fusion, where three independent flow measurement sub-systems and three online calibration/compensation measurements are applied for sub-systems. These are, namely an Electrical Impedance Tomography (EIT) sensor (for measuring dispersed-phase velocity and fraction), an electromagnetic flow metre (EMF, for measuring continuous-phase velocity with an input of the EIT mean volume fraction) and a gradiomanometer flow-mixture density metre (FDM), in addition to on-line water conductivity, temperature and absolute pressure measurements. EIT–EMF–FDM data fusion embedded in the research prototype includes online calibration and compensation, phase fraction decomposition and flow quantity integration.

2.1. Measurement principle

In this work, for a vertical gas-oil–water three-phase (water-continuous) flow, an EIT technique with dual-plane sensors is used to extract local volume fraction distribution, local flow velocity and flow rate of the dispersed phases (e.g. gas and oil) [9]. The online measurement of local volume fraction distribution and profile of the dispersed phases is based on the average of volume fractions of individual pixels, which constitute the entire image. The online measurement of local velocity distribution and profile is based on the pixel–pixel cross-correlation method [11,18,3]. An EMF is used to measure the mean flow velocity and flow rate of water-continuous liquid phase (i.e. water and oil). Recognising the velocity measurement of EMF may have an approximately linearly relation to the volume fraction of dispersed phase in the EMF–EIT combined method ([2,21,4], the velocity shift is treated as a systematic error with other in empirical calibration. Since the EIT provides the combined mean volume fractions of the dispersed phase, it is therefore, necessary to perform online correction of the mean volume fraction of the non-conducting gas and oil phases. The online FDM method [7], which measures the gas–oil–water flow-mixture density (with the gas-phase correction factor provided by an empirical model and an online absolute pressure measurement) is combined with the EIT to determine each constituent phase of oil and gas. It is worth pointing out that in the present work only mean values, obtained from the EIT and EMF, are considered in the calculation, as well as the correction of gas and oil volume fractions. The mean oil volume fraction is determined using the correlation of EIT and FDM, as given in Eq. (1). Knowing the mean volume fraction of oil, the mean gas volume fraction and mean water volume fraction can readily be extracted from the measured volume fraction of the dispersed phases by the EIT, as shown in Eqs. (2) and (3). Therefore, the volume fraction of individual phases can be derived as

$$\bar{\alpha}_O=\frac{(\rho_W-\rho_G)\bar{\alpha}^{EIT}-(\rho_W-\rho^{FDM})}{\rho_O-\rho_G} \tag{1}$$

$$\bar{\alpha}_G=\bar{\alpha}^{EIT}-\bar{\alpha}_O \tag{2}$$

$$\bar{\alpha}_W=1-\bar{\alpha}^{EIT} \tag{3}$$

For vertical water-continuous flows assuming homogeneous flow within the EMF sensing region. Thus, the slip between oil and water velocities can be neglected. Therefore, the velocity of water measured by the EMF can also represent the velocity of oil. The flow rates of each individual phase can be determined as indicated in Eqs. (4)–(6)

$$Q_G=A\bar{\alpha}_G\bar{v}_G^{EIT} \tag{4}$$

$$Q_O=A\bar{\alpha}_O\bar{v}_W^{EMF} \tag{5}$$

$$Q_W=A\bar{\alpha}_W\bar{v}_W^{EMF} \tag{6}$$

where Q, $\bar{\alpha}$, $\bar{v}$ and A are volumetric flow rate, mean volume fraction, mean velocity and the area of pipe cross section respectively; the subscript G, O and W indicate the specific gas/oil/water phase, the superscript denotes the applied sensing technique.

2.2. Three phase volume fractions decomposition

With assumptions of the mixture's density, ρ^{FDM}, and disperse phase fraction (e.g. oil and gas) to be obtained from FDM and EIT respectively, the phase relationship can be presented as

$$\begin{cases}\rho_W\bar{\alpha}_W+\rho_O\bar{\alpha}_O+\rho_G\bar{\alpha}_G=\rho^{FDM}\\ \bar{\alpha}_O+\bar{\alpha}_G=\bar{\alpha}^{EIT}\\ \bar{\alpha}_W+\bar{\alpha}_O+\bar{\alpha}_G=1\end{cases} \tag{7}$$

we have the secondary relationship

$$\rho_O\bar{\alpha}_O+\rho_G\bar{\alpha}_G=\rho^{FDM}-\rho_W(1-\bar{\alpha}^{EIT}) \tag{8}$$

Then, the volume fractions of each phase can be derived as given by Eqs. (1)–(3).

2.3. Calibration and compensations

In EIT, by solving the inverse problem [17], a tomographic image in terms of electrical conductivity contrast is reconstructed using voltage sensing on the peripheral electrodes mounted on the internal surface of the pipe. As formulated in Eq. (9) with an assumption of conductivity of gas and oil to be zero [12], the mean volume fraction of the disperse phase, $\bar{\alpha}_d$ is derived from the conductivity ratio $\bar{\sigma}_m/\sigma_c$, where σ_c is the conductivity of continuous liquid phase (water), $\bar{\sigma}_m$ is the mixture mean conductivity obtained from EIT. $\bar{\sigma}_m$ is independent to the flow pattern [10].

$$\bar{\alpha}_d = \frac{1 - \frac{\bar{\sigma}_m}{\sigma_c}}{1 + 0.5 \times \frac{\bar{\sigma}_m}{\sigma_c}} \tag{9}$$

2.3.1. Flow density metre

As indicated in Eq. (1), the three-phase flow mixture density (ρ^{FDM}) estimated from the gradiomanometer (FDM) is one of the three basic variables along with those measured by EIT and EMF to enable the three phase measurement. Two absolute-pressure sensors are flush-mounted on a straight section of vertical pipe to derive the differential pressure for the determination of the mixture density as well as the absolute pressure for gas density correction. The use of solid-state pressure sensors in this research work avoids the need of liquid-filled pressure-transmitting tubes in a conventional differential pressure sensor. However, the wide measurement range of the chosen absolute pressure sensors may cause a low sensitivity and therefore a marked measurement error for the derived differential pressure (DP) measurement. A specific differential amplifier is designed with high common voltage rejection ratio to enhance the performance of the DP signal. The DP sensor is calibrated to correct the offset over the full measurement range. Taking into account the effects of frictional pressure loss, the mixture density ρ_{FDM} can be estimated from the following equation:

$$\rho^{FDM} = \frac{\Delta P^{FDM}}{h\left(g + \frac{2C_f v^2}{D}\right)} \tag{10}$$

where ΔP^{FDM} is the measured gradio differential pressure, v the liquid velocity, D the pipe diameter, h the distance between the two pressure sensing points, g the gravitational acceleration constant, C_f the Fanning friction factor with the Reynolds number being $Re = \rho_l v D/\mu$. where ρ_l, μ are the continuous phase (water) dynamic density and viscosity, respectively. Besides Eq. (9), the volume fraction of the dispersed phase α_d (e.g. oil or gas) can be deduced alternatively, for a water-continuous two-phase flow, as

$$\alpha_d = \frac{\rho^{FDM} - \rho_w}{\rho_d - \rho_w} \tag{11}$$

where ρ_d and ρ_w are the densities of dispersed phase and water, respectively.

2.3.2. Calibration

Eq. (9) is rearranged into Eq. (12) that indicates how the conductivity ratio $\bar{\sigma}_m/\sigma_c$ can be deduced from the known volume fraction α_d.

$$\frac{\bar{\sigma}_m}{\sigma_c} = \frac{2(1 - \alpha_d)}{2 + \alpha_d} \tag{12}$$

when the volume fraction α_d is acquired from FDM using Eq. (11), the conductivity ratio σ_m/σ_c is simply corrected by the calibration coefficient, η, at any measurement stage with no requirement of the conductivity reference at zero volume fraction, which is presented in Eq. (13).

$$\eta \cdot \frac{\bar{\sigma}_m}{\sigma_c} = \frac{2(1 - \alpha_d)}{2 + \alpha_d} \tag{13}$$

2.3.3. Compensations

In multiphase flow measurement, the conductivity of the water-continuous liquid phase may change due to variations in the water temperature and/or salinity (ionic concentration). To obtain robust phase fraction distributions reconstructed by the use of linear back projection algorithm, it is therefore necessary to apply online compensation to the conductivity readings of the continuous water phase. Two methods are embedded in the flowmeter research prototype, which are selectable depending on whether the change is due to the salinity or due to the temperature, based on the measurements from either an online water-conductivity cell (Eq. (14)) or temperature sensor (Eq. (15)) respectively. Since only the relative change of conductivity is used in the data fusion, the actual value of conductivity is less important. The deviation of conductivity due to the relative change of either temperature or ionic concentration is used for measurement compensation in the system.

$$\sigma_c = k \cdot \sigma_0 \tag{14}$$

or

$$\sigma_c = (1 + \lambda \Delta T) \cdot \sigma_0 = \beta \cdot \sigma_0 \tag{15}$$

where σ_0, λ and ΔT are the original conductivity of the continuous phase, temperature coefficient and change of temperature at the time taking the reference voltage measurement, k is the conductivity cell constant in case of using the online conductivity cell and $\beta = (1 + \lambda \Delta T)$.

Combining all the above effects, the calibration and compensation can be made by Eqs. (16) or (17), depending on the source of the change and the suitability in practise.

For compensating the conductivity change due to the change of ionic concentration and/or temperature

$$\alpha_d = \frac{1 - \frac{\eta \bar{\sigma}_m}{k\sigma_0}}{1 + 0.5 \times \frac{\eta \bar{\sigma}_m}{k\sigma_0}} \tag{16}$$

For compensating the conductivity change only due to the change of fluids' temperature

$$\alpha_d = \frac{1 - \frac{\eta \bar{\sigma}_m}{\beta\sigma 0}}{1 + 0.5 \times \frac{\eta \bar{\sigma}_m}{\beta\sigma 0}} \tag{17}$$

The correctness of both absolute and differential pressures is important. They may be calibrated by a set-up with or without a liquid having known density in the system. The absolute pressure and temperature measurement are also necessary to compensate the gas flow rate to the standard value at the room temperature (20 °C) and at the ambient pressure (1 bar).

2.4. Measurement system

The research-prototype three-phase flow measurement system is illustrated as Fig. 1, which is consists of an EIT (ITS V5r EIT system) with a dual-plane sensor [9], an EMF flow metre (OPTIFLUX 4000, from KROHNE), two absolute pressure sensors (PXM209-2.50A10V, from OMEGA), one temperature sensor (RTD-NPT-72-E-MTP-M, from OMEGA) and an in-house-build online conductivity cell. A photograph and line sketch of the integrated sensor is given in Fig. 2. Computer software with graphic interface is used for control of data collection, online data fusion and display.

3. Two- and three-phase flow measurements

The flow-measurement experiment was conducted on the inclinable multiphase flow facility at Schlumberger Gould Research, Cambridge (SGR), UK). Tap water, kerosene oil and nitrogen gas were used as the test fluids. The test included a large number of

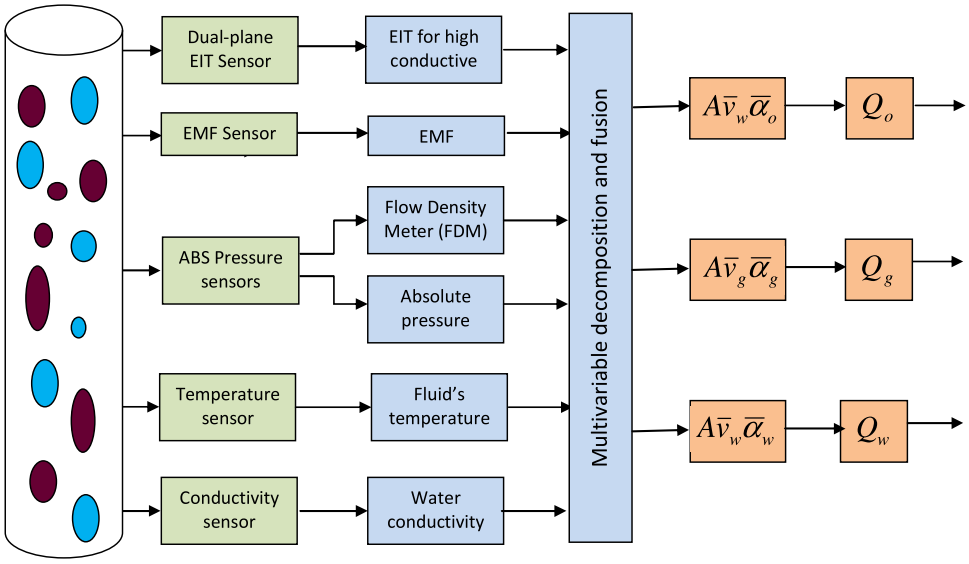

Fig. 1. The prototype three-phase flow measurement.

combinations of flow conditions, mostly for vertical upward pipe flows, with range of water flow rate (q_W) 0.5–15 m^3/h, oil flow rate (q_O) 0.5–10 m^3/h, and gas flow rate (q_G) 0–42 m^3/h, which made the range of gas volume fraction (GVF)= 0–97% [GVF= $q_G/(q_G+q_O+q_W)$]. The tests covered oil/water two-phase flows with Water Cut (WC)= ~30– 100% [WC= $q_W/(q_O+q_W)$]; oil/water/gas three-phase flows with similar WC and GVF ranges at line pressure up to 2.2 bar. For vertical upward high-flow rate oil/water flows, the velocity slip between the oil and water phases is considered to be negligible. Note that WLR= $\alpha_W/(\alpha_O+\alpha_W)$. Hence WLR=water cut when there is no oil–water velocity slip ($v_w=v_o$). Measurement scope of the prototype system is for vertical oil-in-water, gas-in-water or gas-oil-in-water flows.

3.1. *Online visualisation of measurement results and dispersed phase*

In order to visually present measurement results, the software offers user-friendly graphic interface to demonstrate the intermediate and final outcomes of online computation. Fig. 3 depicts overall visualisation of computational results by the software for oil-in-water 2-phase and gas-oil-in-water 3-phase upward flows. In Fig. 3a, concentration and velocity profiles of dispersed (oil) phase are presented as upper-left 2 plots, below which is the disperse phase flowrate. The right part of the picture shows the mean concentration, velocity, and flowrate of the continuous (water) phase. Similar to Fig. 3a, Fig. 3b contains concentration and velocity profiles (2 plots), but it combines instantaneous results of

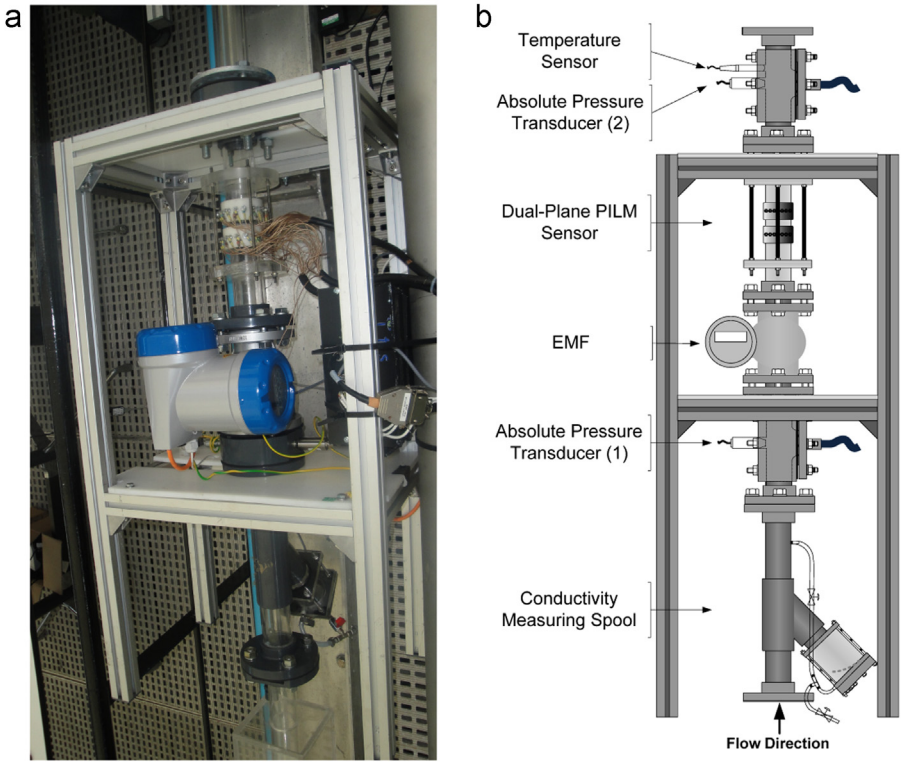

Fig. 2. Photograph (a) and line sketch (b) of the integrated measurement system.

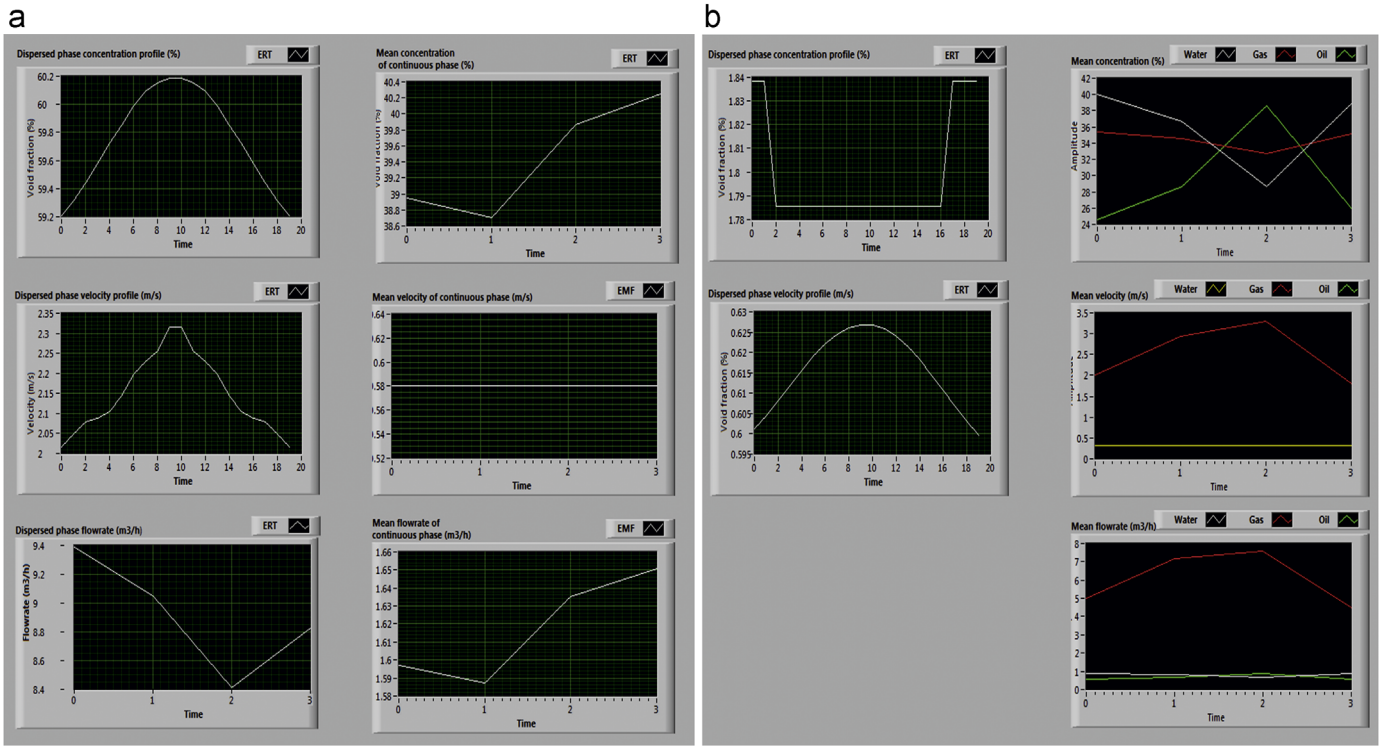

Fig. 3. Screenshots of visual presentation of measurement results for (a) oil-in-water two-phase flow and (b) gas-oil-in-water three-phase flow.

each phase together to 3 different plots for concentration, velocity, and flowrate, respectively, (the right part of the Fig. 3b).

In addition to the visual presentation of measurement results, flows are visualised with different flow conditions as well, by means of accumulating diameter-direction pixels of cross-sectional concentration tomograms from 2000 frames to form axial cross-sectional stacked images. Shown in Fig. 4a and b demonstrates the axial stacked images of oil-in-water flow, and Fig. 4c–e demonstrates the images of gas-oil-in-water 3-phase flow. From flow pattern point of view, Fig. 4 also indicates different flow regimes, including bubbly flow (Fig. 4a and c), transition between bubbly flow and slug flow (image 4b), and slug flow (Fig. 4d and e).

3.2. *Oil–water two-phase measurements*

Fig. 5 illustrates the comparison results of measured mean oil-in-water two-phase flow with that of the reference. Since oil and water are incompressible fluids, therefore, the inlet conditions (i.e.

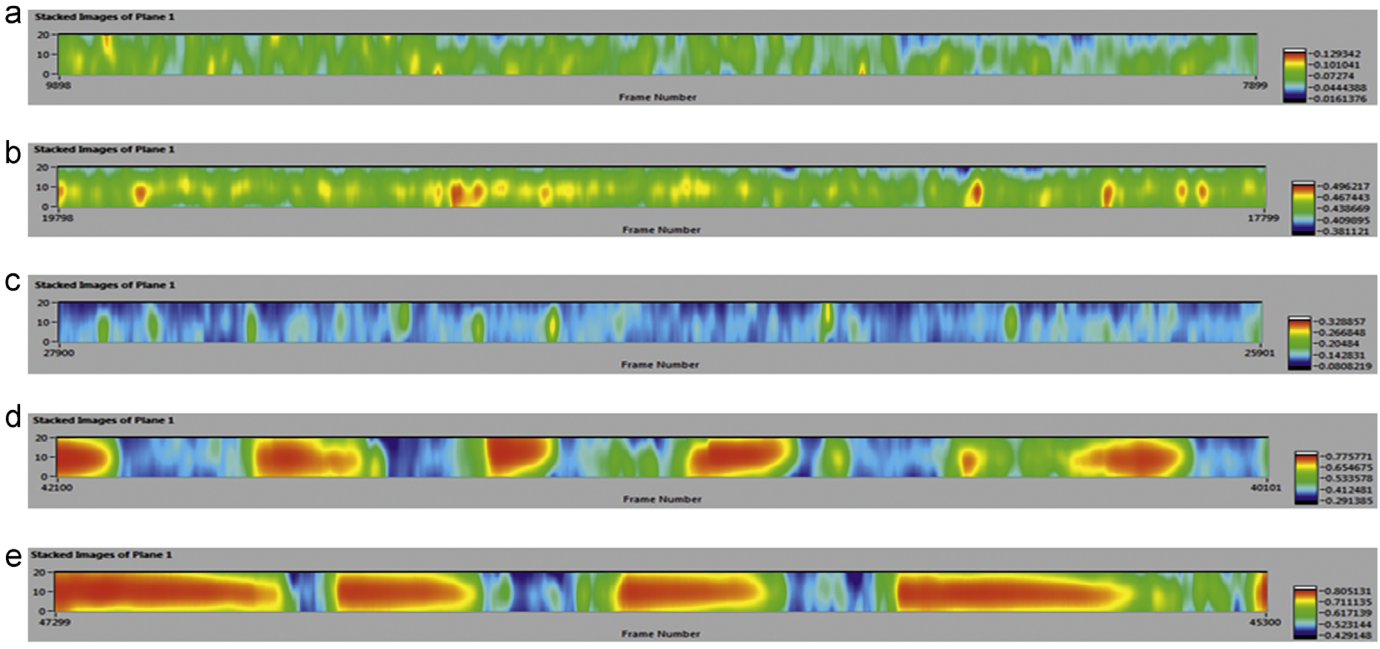

Fig. 4. 2000 frames axially stacked images of different flow patterns, (a) oil-in-water with oil flowrate of 1 m^3/h and water flowrate of 11 m^3/h, (b) oil-in-water with oil flowrate of 6 m^3/h and water flowrate of 6 m^3/h, (c) gas-oil-in-water with gas flowrate of 2 m^3/h, oil of 2 m^3/h, and water of 15 m^3/h, (d) gas-oil-in-water with gas flowrate of 10 m^3/h, oil of 2 m^3/h, and water of 5 m^3/h, and (e) gas-oil-in-water with gas flowrate of 15 m^3/h, oil of 2 m^3/h, and water of 2 m^3/h.

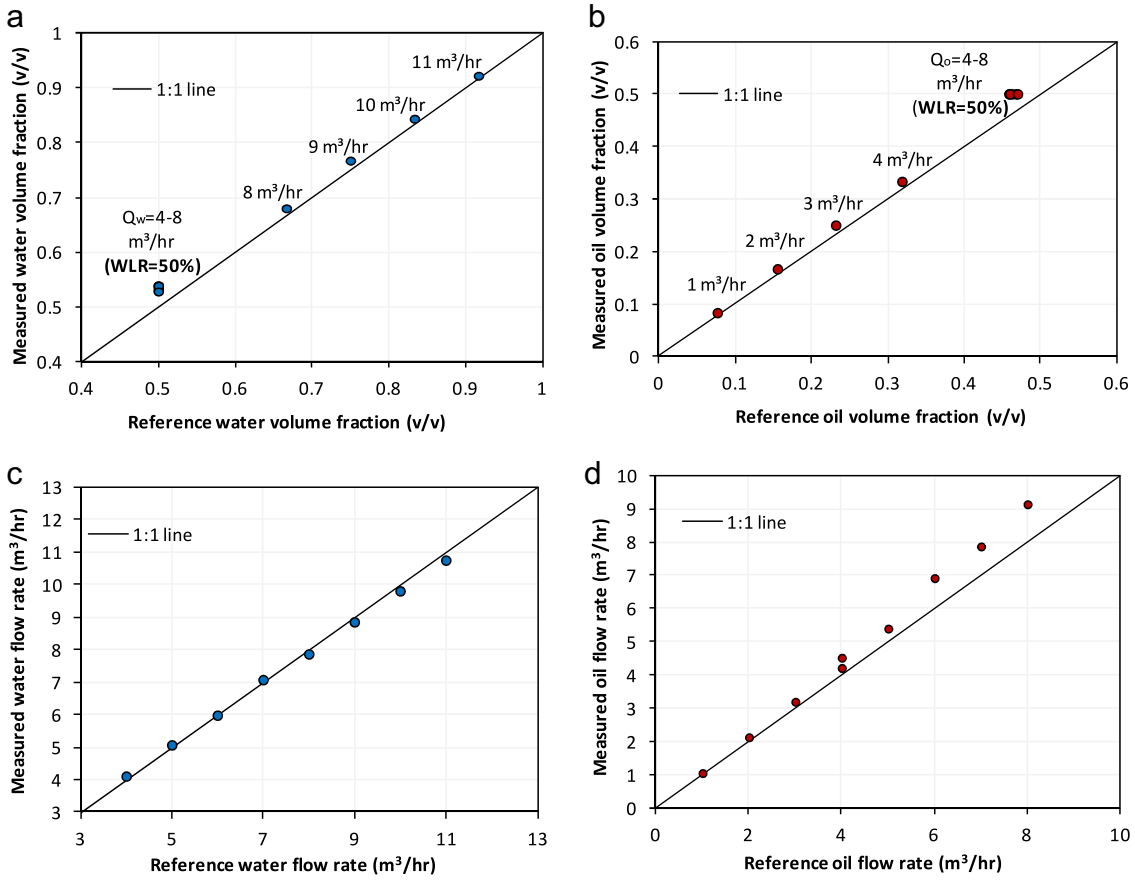

Fig. 5. Comparison results of measured oil-in-water two-phase flow with that of reference: (a) water volume fraction, (b) oil volume fraction, (c) water flow rate, and (d) oil flow rate.

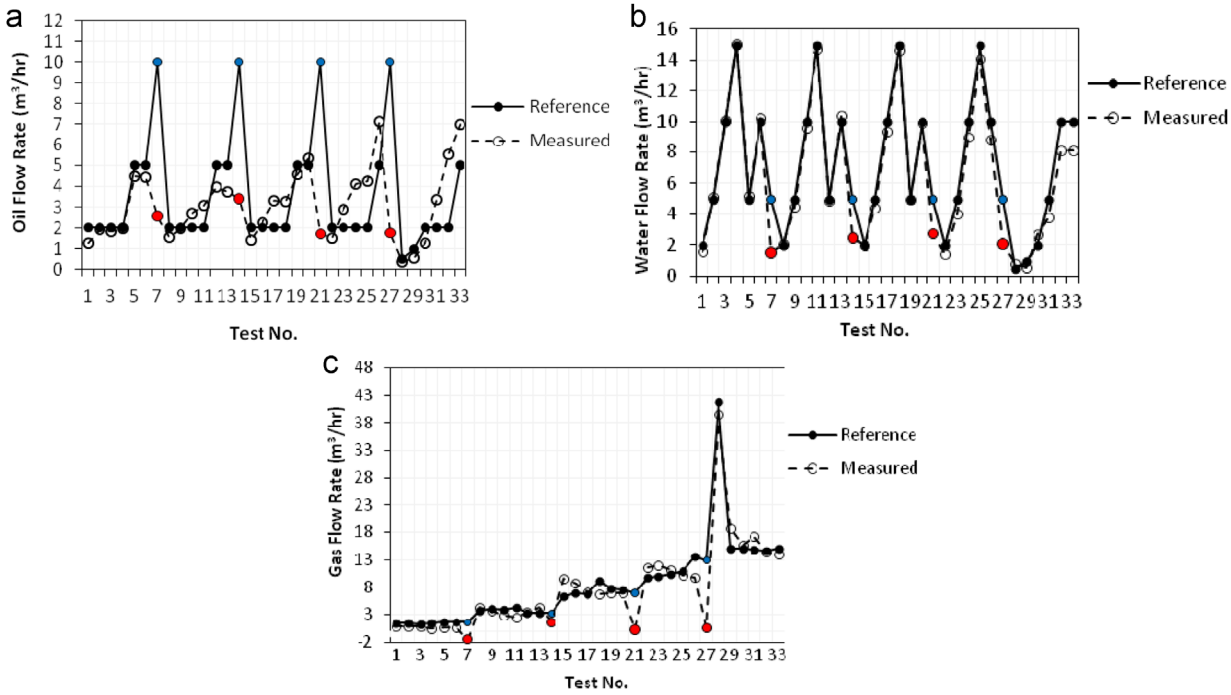

Fig. 6. Overall results of gas-oil-water three-phase flow measurement for 33 flow conditions: (a) oil flow rate, (b) water flow rate, and (c) gas flow rate.

flow velocity and volume fractions) can be used for the purpose of comparison with the measured values. By observing Fig. 5b, it is apparent that the deviation of the EIT-measured oil volume fraction from the non-slip reference value increases with increasing oil volume fraction. Since the water volume fraction is obtained from the EIT-measured mean oil volume fraction, similar

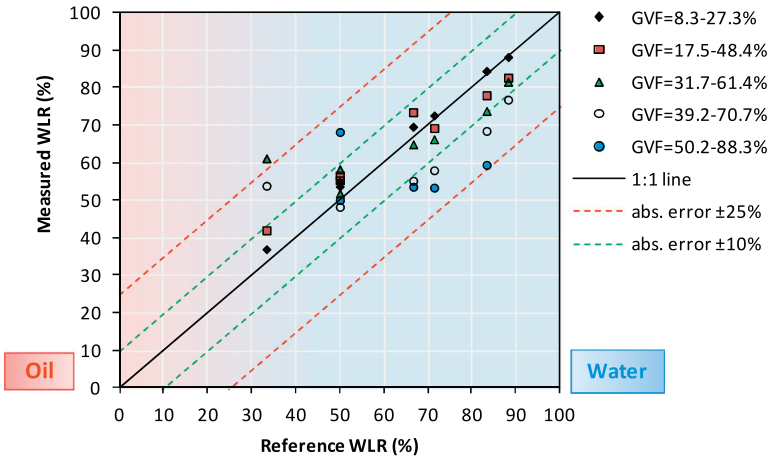

Fig. 7. The measured WLR compared with the reference for different range of GVFs (with the ±10% and ±25% absolute-error boundaries shown).

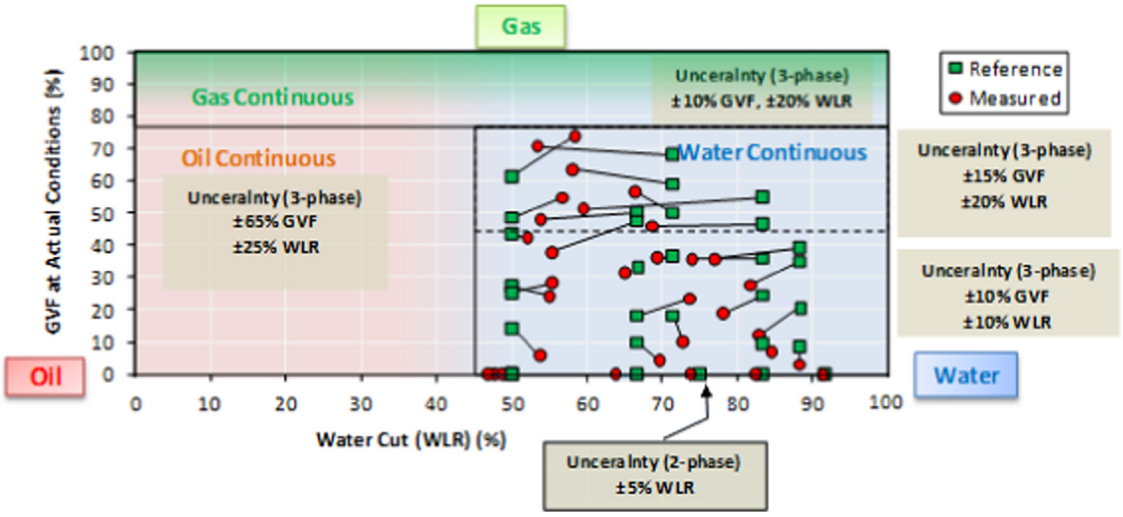

Fig. 8. GVF-vs-WLR Composition map summarizing the research-prototype measured GVF and WLR compared with the respective references, for two- and three-phase vertical upward flow within water-continuous region.

deviation is mirrored in the measured water volume fraction (Fig. 5a). For oil–water flow rate measurement, Fig. 5d shows an increasing over-estimation of the measured oil flow rate relative to the reference, with the increase in the oil flow rate. The measured water flow rate (with the mean water velocity derived from the EMF), on the other hand, largely closely follows the flow-loop reference (Fig. 5c). By observing the mean oil volume fraction, which is extracted from the EIT, it can be seen that by further approaching the phase-inversion (33% for low viscosity kerosene) further deviation in the measured values can be noticed. Since the mean water volume fraction is also determined from the EIT, similar deviation is reflected in the trend of mean water volume fraction. This deviation is particularly pronounce for the conditions WLR=50%, which is quite close to the phase-inversion value. On the other hand, it is quite apparent that this deviation is still reflected in the measured oil flow rate, but not in the measured water flow rate. Since the volume fraction of both phases is extracted from the EIT, if the error is attributed to the measured volume fractions, then it should also reflect in the measured flow rates of both constituent phases. Therefore, a conclusion can be drawn that, although some error can be remarked in the measured volume fractions obtained from the EIT, the source of error is not predominantly coming from the measured phase volume fractions. It can be concluded that the large deviation in the measured oil flow rate is attributed to the error in the mean oil velocity obtained by the EIT pixel-wise cross-correlation. Since the relative error $\delta V_L/V_L = -\delta\tau/\tau = -(V_L/L)\delta\tau$; with transit-time resolution $\delta\tau$=1 ms, V_L=1.2–2.4 m/s, dual-plane spacing L=50 mm, $\delta V/V$=−2.4% to −4.8% (In the oil–water flow test results shown here, there is no assumption of an equal mean velocity between the oil and the water phases).

3.3. Gas-oil-water three-phase measurements

The overall measurements, including the reference measurements from SGR for 33 flow conditions are summarised by Fig. 6. All the measurements were carried out within water continuous region with WLR >50%, except for four test conditions, which were carried out within oil continuous region (WLR=33%). The phase-inversion WLR for low viscosity kerosene and water mixture is around 35%. These four conditions are highlighted by blue-colour data points as reference values and the corresponding measured values are represented by red-colour data points. It is quite clear that a reasonable agreement with the references can be observed for all the measured flow rates within water continuous region. However, for the measured flow rates of oil continuous flows a very large deviation from the reference is apparent. By observing the trend of measured oil flow rates, it can be seen that the level of deviation is more pronounced than that of the measured water flow rate and that of the measured gas flow rates; the

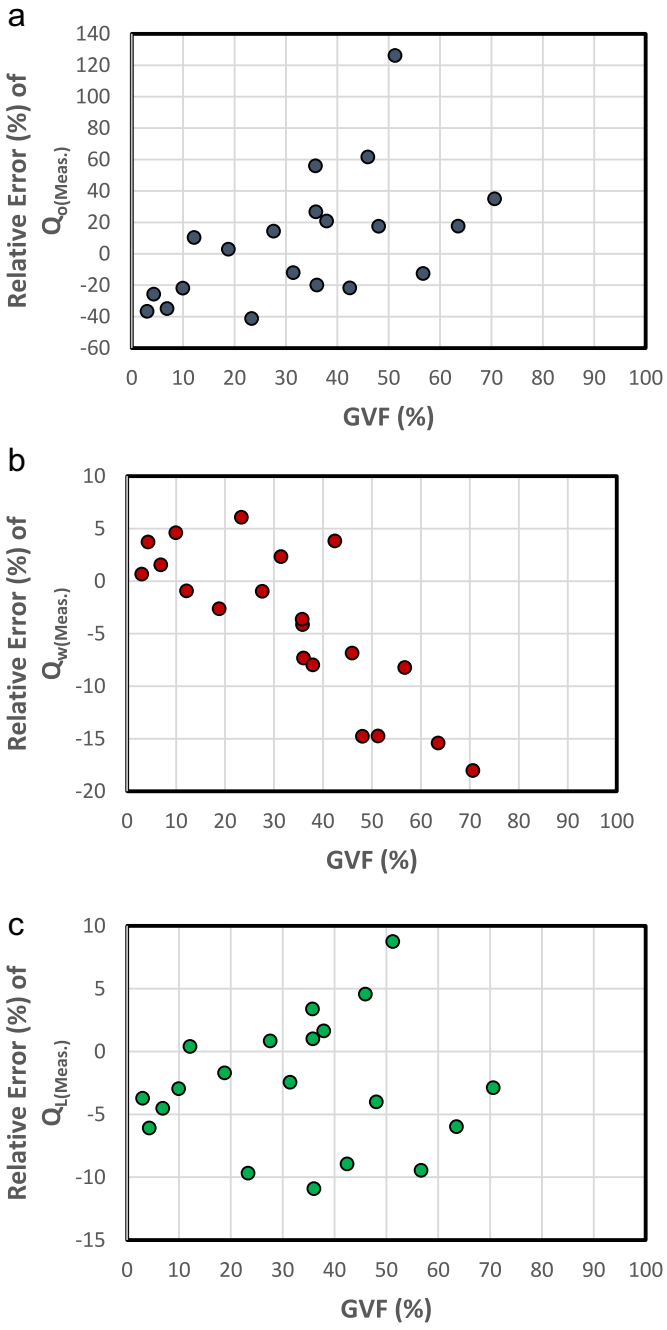

Fig. 9. Ratios of the measured to the reference liquid phase flow rates vs. GVF: (a) oil flow rate, (b) water flow rate and (c) liquid flow rate.

deviation grows more with the increase of oil flow rate. On the other hand, the comparison results of gas flow rate between the measured and reference values suggest that higher deviation in the oil flow rate is associated with higher gas flow rates, as shown in Fig. 6c. The possible reason for this is that the higher gas flow rate does not allow the existence of a water-rich conductive-layer around the EIT electrodes that are flush-mounted with the pipe wall.

To further illustrate the uncertainties in the flow-measurement and identify the operating region in terms of WLR and GVF, the comparison between the estimated WLR and the reference WLR is shown in Fig. 7. It is can be seen that, within the range of 45–100% WLR and the range of GVF 0–45%, the estimated WLR has an absolute-error within $\pm$ 10%.

Fig. 8 presents all the results obtained from two- and three-phase vertical upward flow tests carried out in SGR, as a GVF-vs-WLR composition map, with water-continuous and oil-continuous regions indicated, in blue and red colours, respectively. The boundary of oil-and water-continuous regions is shown at WLR = 45% as an example. The gas continuous flow region is roughly illustrated as being between 78–100% GVF. In the composition map the reference and measured WLR is plotted against the reference and measured GVF. The reference values are highlighted in green data points, while the measured values are represented by red ones. Each measured value is connected to the corresponding reference value through a straight line, with its projected lengths in the WLR-axis and GVF-axis indicating the discrepancies (in absolute-error in percentage) in the WLR and GVF, respectively. It can be seen that the measurements of two-phase (oil-in-water) flow, which are distributed along the *x*-axis within water continuous region, have an uncertainty of $\pm$ 5%. On the other hand, the measurements for three-phase flow have $\pm$ 10% uncertainty in WLR and GVF within the water-continuous region (45–100% WLR) and within the GVF range of 0–45%. The performance of the WLR and GVF measurement deteriorates for GVF > 45%, where the WLR-error doubles. It is worth pointing out that any measurement carried out near the oil-continuous region (33% WLR) is associated with an uncertainty of $\pm$ 65% GVF and $\pm$ 25% WLR, due to that the EIT-based measurement is limited to water-continuous flow only.

The flow-rate measurement relative errors of oil, water and liquid, are given in Fig. 9 versus the GVF. The references were obtained from SGR flow facility. Fig. 9a shows that the relative error of the oil flow rate increases up to 120% with increasing GVF. The relative error of the water flow rate is up to about 20% at GVF = 70%, but within 10% for GVF $<$ ~45% (Fig. 9b). However, the relative error of the total liquid flow rate is largely around 10% (Fig. 9c). Further research is needed to fully understand the source of these flow-rate measurement errors.

4. Conclusions

This paper presented initial gas-oil-water three-phase flow measurement results from an Electrical Impedance Tomography combined with an electromagnetic flow metre and a gradiomanometer flow-mixture density metre, and with online water-conductivity and temperature sensors. The results of oil-in-water two-phase flow measurement, obtained from the combination of EIT and EMF, has also been demonstrated. The targeted measurement is limited to vertical upward flow with water continuous flow. It can be concluded that the measurements of two-phase (oil and water) flow have an uncertainty of $\pm$ 5%, which will be much better than $\pm$ 5% after a linear correction is applied [6]. For three-phase flow measurement, the results indicate that the error of the measured water flow rate is within $\pm$ 10% when the flow is water continuous (i.e. when liquid has a higher WLR > 45%) and of moderate GVF (GVF < ~45%). The error of the estimated oil flow rate is within $\pm$ 10% when the flow has a WLR > 45% and a moderate GVF < ~45%. The measured oil flow rate has a pronounced deviation more than that in the measured water flow rate and gas flow rate. The deviation is further increased with increase of oil flow rate to a point where a larger deviation can be noticed, which is again, similar to estimated water flow rate; the high measurement error is generated within the oil continuous region (WLR < 33%). The measurement errors increase with the increase of GVF, which may be due to the limited capacity of EIT in handling the high-fraction of dispersed (oil and gas) phases, as well as the limited imaging spatial resolution from the dual-plane 8-electrode sensor used. The short time duration of EIT data sampling (to represent the steady state of flow) would be other source of errors. It

could also be due to the 'malfunctioning' of the FDM method for a high GVF non-homogeneous flow, the lack of desired stability of differential-pressure measurement from two absolute pressure sensors.

Further work to improve the performance of the prototype system is ongoing, including calibration, slip velocity correction and flow regime assessment, improved FDM method and modelling, enhanced EIT imaging resolution and sampling rate.

Acknowledgements

The work described in this paper has been funded by the Engineering and Physical Sciences Research Council (EP/H023054/1), UK, with the academic collaborators being University of Cambridge, University of Huddersfield and industrial partners being Schlumberger Gould Research, Industrial Tomography Systems and National Engineering Laboratory.

References

[1] M. Appel, J.J. Freeman, D. Pusiol, Robust multi-phase flow me asurement using magnetic resonance technology, in: Proceedings SPE Middle East Oil and Gas Show, Manama, Bahrain, September 2011 (SPE 141465).
[2] J.E. Cha, Y.C. Ahn, M.H. Kim, Flow measurement with an electromagnetic flowmeter in two-phase, Flow Meas. Instrum. 12 (2002) 329–339.
[3] X. Deng, F. Dong, L.J. Xu, X.P. Liu, L.A. Xu, The design of a dual-plane EIT system for cross correlation measurement of bubbly gas/liquid pipe flow, Meas. Sci. Technol. 12 (2001) 1024–1031.
[4] X. Deng, G. Li, Z. Wei, Z. Yan, W. Yang, Theoretical study of vertical slug flow measurement by data fusion from electromagnetic flowmeter and electrical resistance tomography, Flow Meas. Instrum. 22 (2010) 272–278.
[5] G. Falcone, G.F. Hewitt, C. Alimonti, B. Harrison, Multiphase flow metering: current trends and future development, The SPE 2001 Annual Technical Conference and Exhibition, Society of Petroleum Engineers, New Orleans, SPE 74689, 2002.
[6] Y. Faraj, M. Wang, J. Jia, Q. Wang, C.G. Xie, G. Oddie, K. Primrose, C. Qiu, Measurement of vertical oil-in-water two-phase flow using dual-modality ERT/EMF system, in: Proceedings of the 5th International Workshop on Process Tomography, Jeju, South Korea, 2014.
[7] E.J. Fordham, C.P. Lenn, A. Holmes, S. Simonian, R.T. Ramos, Corrections of gradiomanometer data for volume fractions in two-phase flows, Meas. Sci. Technol. 10 (1999) 131–135.
[8] D.L. George, J.R. Torczynski, K.A. Shollenbeger, T.J. O'hen, S.L. Ceceio, Validation of electrical-impedance tomography for measurements of material distribution in two-phase flows, Int. J. Multiph. Flow 26 (2000) 549–581.
[9] J. Jia, M. Wang, H.I. Schlaberg, H. Li, A novel tomographic sensing system for high electrically conductive multiphase flow measurement, Flow Meas. Instrum. 21 (2010) 184–190.
[10] J. Jia, M. Wang, Y. Faraj, Evaluation of EIT systems and algorithms for handling full void fraction range in two-phase flow measurement, Meas. Sci. Technol. 26 (1) (2015).
[11] G.P. Lucas, J. Cory, R. Waterfall, W.W. Loh, F.J. Dickin, Measurement of the solids volume fraction and velocity distributions in solids–liquid flows using dual-plane electrical resistance tomography, J. Flow Meas. Instrum. 10 (4) (1999) 249–258.
[12] J.C.A. Maxwell, 5rd edition,Treatise on Electricity and Magnetism, vol. 1, . Dover Publications Inc., New York, 1873.
[13] V. Mosorov, D. Sankowski, L. Mazurkiewicz, T. Dyakowski, The 'best-correlated pixels' method for solid mass flow measurements using electrical capacitance tomography, Meas. Sci. Technol. 13 (2002) 1810–1814.
[14] M. Sharifi, B. Young, Electrical Resistance Tomography (ERT) applications to chemical engineering, Chem. Eng. Res. Des. 91 (9) (2013) 1625–1645, http://dx.doi.org/10.1016/j.cherd.2013.05.026.
[15] R. Thorn, G.A. Johansen, B.T. Hjertaker, Three-phase flow measurement in the petroleum industry, Meas. Sci. Technol. 24 (012003) (2012) 17.
[16] H. Van Santen, Z.I. Kolar, A.M. Scheers, Photon energy selection for dual energy γ- and x-ray absorption composition measurements in oil–water–gas mixture, Nucl. Geophys. 9 (1995) 193–202.
[17] M. Wang, Inverse solutions for Electrical Impedance Tomography based on conjugate gradients methods, Meas. Sci. Technol. 13 (1) (2001) 101–117.
[18] M. Wang, Y. Ma, N. Holliday, Y. Dai, R.A. Williams, G. Lucas, A high performance EIT system, IEEE Sens. J. 5 (2) (2005) 289–299.
[19] C.G. Xie, I. Atkinson, C. Lenn, Multiphase flow measurement in oil and gas production, in: Proceedings of the 5th World Congress on Industrial Process Tomography, vol. 3–6, September 2007, pp. 723–736.
[20] T. York, Status of electrical tomography in industrial applications, J. Electron. Imaging 10 (3) (2001).
[21] J.Y. Xu, Y.X. Wu, Z.C. Zheng, M. Wang, Measurement of solid slurry flow via correlation of electromagnetic flow meter, electrical resistance tomography and mechanistic modelling, J. Hydrodyn. 21 (4) (2009) 557–563.